MORPHOLOGICAL CONTROL OF MULTIFUNCTIONAL MELTING GEL COATINGS VIA ELECTROSPRAY DEPOSITION

By

ARIELLE MARIE R. GAMBOA

A thesis submitted to the

School of Graduate Studies

Rutgers, the State University of New Jersey

In partial fulfillment of the requirements for the degree of

Master of Science

Graduate Program in Mechanical and Aerospace Engineering

Written under the direction of

Jonathan P. Singer

And approved by

_____

_____

_____

New Brunswick, New Jersey

May 2020

ABSTRACT OF THE THESIS

Morphological Control of Multifunctional Melting Gel Coatings via Electrospray Deposition

By ARIELLE MARIE R. GAMBOA

Thesis Director:

Jonathan P. Singer

Melting gels are a class of hybrid organic-inorganic gels prepared via the sol-gel process that have glass transition temperatures near room temperature and consolidation temperatures ~150°C. Their thermal properties allow for useful processing techniques: melting gels exhibit thermoplastic behavior below their consolidation temperatures, then undergo complete cross-linking to form organically modified silica networks upon consolidation. By appropriately tuning surface properties, these glass sprays can be used as protective coatings in electronics and anti-corrosion in metals. Electrospray deposition was used to spray dilute solutions of 1 wt% melting gels in 2-butanone onto silicon substrates. Electrospray uses high voltages to produce charged, monodisperse droplets, and because of the low solid contents used in our study, it uniformly delivers small amounts of melting gel at a continuous rate. Parameters such as the pH of melting gel synthesis, solution viscosity, and spray polarity can be varied to alter and study the effects of charge injection on the consolidation of the melting gel into hybrid glasses. Optical images, film thickness measurements, nanoindentation, FT-IR, and goniometry were used to evaluate and demonstrate the effects of these variables on both the physical morphology along with the chemical structure of the final coatings.

ACKNOWLEDGMENTS

To my parents, family, friends, and colleagues. Your contribution to this work was immeasurable, and I am eternally grateful.

To my advisor, Professor Jonathan P. Singer, for all his guidance and mentorship throughout this journey. He has been a mentor to me since my first year here, and I have learned so much during my time in this group.

To Professor Andrei Jitianu at the Department of Chemistry at Lehman College, City University of New York, for all his guidance as I navigated a new field of collaborative research.

To the other members of our research group – Lin Lei, Tianxing Ma, Robert Green-Warren, Dylan Kovacevich, Christianna Kuznetsova, Michael Grzenda, Yogin Patel, and Kyle Buznitsky – for all their support for this work.

To dear friends and former colleagues Valeria Saro-Cortes and Michael Nitzsche, for their continued support and encouragement.

This work was supported by the Advanced Manufacturing Program of the National Science Foundation through award no. 19111518.

Table of Contents

List of Figures

List of Tables

1. Introduction

The ability to manipulate surface properties by adding controlled coatings is an important area of materials processing. By altering surface micro- and nanostructure, the nature of the surface's interactions with the surroundings is affected, bringing about important implications in design and longevity. Enabling durable ceramic coatings in a way that provides control over the functionality of that film opens up a wealth of applications to be explored. As a motivating example, Figure 1 shows a preliminary result of a bilayer CMG coating generated using processing parameters designed to arrive at a dense bottom layer and tenuous, superhydrophobic top layer. Such a coating could act as both an anti-fouling surface and an anti-corrosive barrier, manufactured without the need for expensive or time-consuming: (1) thermal post-treatment of particle spray, (2) vacuum deposition of CVD or ALD, and (3) aging or lengthy annealing and (4) freeze/super-critical drying of sol-gel films. These advances represent considerable decreases in tooling and processing cost. Further, by adding a new set of low-temperature substrates such as hydrogels, other applications in a biomedical context, such as biocompatible surfaces that possess controlled corrosion (i.e. biodegradation) mechanisms, become possible. Lastly, electrospray deposition (ESD) is one of the most viable routes to attaining microscale morphological control on **3D surfaces** in ambient conditions. Past work [10] has shown that ESD can produce a 2-45 μm thick

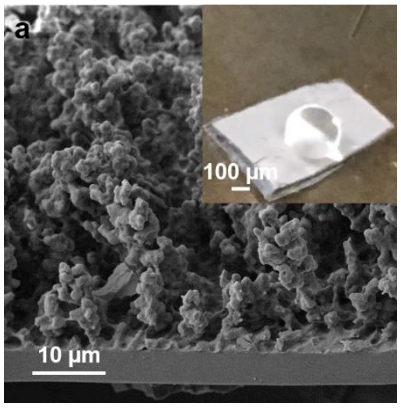

Figure 1: 45° - angled SEM image of a bilayer consolidated melting gel coating on a silicon wafer formed by electrospray deposition

conformal 3D coating of consolidated melting gel on a statue. A coating with this level of smoothness in a composite material would be impossible to produce through any other single deposition process. As will be discussed, deposition of this coating required control of the viscosity and temperature of the spray. The degree of structural control and the compatibility with various substrates are dependent on a number of factors that need to be explored. Electrospray deposition is an electrostatic phenomenon by nature, and this charge has an effect on the consolidation mechanism of melting gel materials. Furthermore, the buildup of film during deposition may also alter both processes' thermodynamics and kinetics. Finally, charge dissipation mechanisms are influenced by viscosity, so the dilution and blending of porogens and nanoparticles into melting gels not only affect their rheological properties but also their final electrosprayed structures. These interactions merit investigation, and in doing so results will allow further control of consolidated melting gel properties according to their desired applications.

1.1 Melting Gels

1.1.1 OSS Melting Gels

Oligomeric silsesquioxanes, or melting gels, are hybrid organic-inorganic gels comprised of an inorganic 3D network with functional organic components. Melting gels were first introduced by Matsuda et al. in 2001 [15]. They investigated the formation of poly(benzylsilsesquioxane) particles deposited onto an ITO substrate by electrophoretic deposition. After heat treatment, continuous and uniform transparent thick coatings were obtained. The process called "melting" is a softening process that occurs by sufficiently exceeding the glass transition temperature, T_g. Since the advent of its creation, melting gel

processing techniques have evolved and allowed for the formation of gels with a range of compositions.

The combination of organic and inorganic components into a homogenous, single-phase matrix allows for the fine-tuning of gels mechanical, electrical, and optical properties as required by desired applications. For instance, as electrochemically inert composites, melting gels have proven useful as substitutes to sealing glasses in electrical components [17]. Their hybrid composition combines the advantages of both organic (e.g. organic polymers) and inorganic (e.g. inorganic glasses) alternatives, specifically low temperature sealing (< 200 °C) that is compatible with batteries and hermeticity for effective protection against unwanted vapors. Experiments with two melting gel compositions showed no cracking during the preparation process, low helium permeability comparable to typical seals, and successful prevention of solvent leaks. Methyl-substituted melting gels have also been used as anti-corrosion coatings on AISI 304 stainless steel [2], titanium alloy [3], and magnesium [4]. Strong covalent bonding provides melting gels good adhesion to their coating substrates, and the sol-gel process allows for the formation of dense, crack-free films. The melting gels exhibited some degree of plastic behavior during scratch tests, and they showed no signs of degradation after simulating corrosion wear in salt solutions.

1.1.2 Synthesis via the Sol-Gel Process

The sol-gel process refers to the initiation of an inorganic network out of solution. It involves the use of a colloidal solution ("sol") to generate a gel network of interconnected pores and particles. Its use as a processing technique for inorganic ceramics and glasses has been studied as early as the 19th century and has since emerged as a major means to produce hybrid silica gels. This versatile method is frequently used for the preparation of

a large spectrum of materials from nanocomposites to monoliths. Its importance as a coating method is evident in its use in the production of antireflection coatings of silica [5] and indium tin oxides (ITO) [6]. Unlike traditional methods used in the synthesis of gels, such as glass melting or ceramic powder techniques, the sol-gel process is a low-cost and low-temperature technique, and it also provides higher purity and homogeneity in the resulting gels. One of the most important and unique features of this method is the ability to prepare hybrid organic-inorganic materials by incorporating or bonding organic moieties or molecules to the inorganic networks. Hybrid organic-inorganic materials made by the sol-gel process are not simple blends—they possess the synergistic trends of physical and chemical properties, which are significantly different from mixing models of the individual components.

The formation of a sol-gel monolith can arise from the gelation of a colloidal solution or from the hydrolysis and polymerization of alkoxide precursors. The former approach generates a network of particles from discrete colloids while the latter produces an interconnected 3D network. Melting gels have typically been synthesized using the latter approach, beginning with a variety of organometallic precursors such as tetraethyl orthosilicate (TEOS) and mono- or di-substituted siloxanes, which then produce composites with components mixed at the nanoscale. These siloxane substitutes do not hydrolyze during the sol-gel process, and this incomplete formation of the 3D network lends melting gels their characteristic “melting” or softening behavior. The nanoscale mixing phenomenon provides an important fine control of the gel’s chemical composition that allows for the selection of macro-scale properties depending on desired applications. After the formation of the inorganic backbone via gelation and drying, the net result is a

stable hybrid organic-inorganic gel with functional groups. Table 1 and Figure 2 show typical siloxanes used in the synthesis of melting gels.

TABLE 1: Reagents used to synthesize the relevant melting gels in this study

Reagent	Abbreviation	Chemical Formula
Methyl triethoxysilane	MTES	$C_7H_{18}O_3Si$
Dimethyl diethoxysilane	DMDES	$C_6H_{16}O_{2a}Si$
Phenyl triethoxysilane	PhTES	$C_{12}H_{20}O_3Si$
Diphenyl diethoxysilane	DPhDES	$C_{16}H_{20}O_2Si$

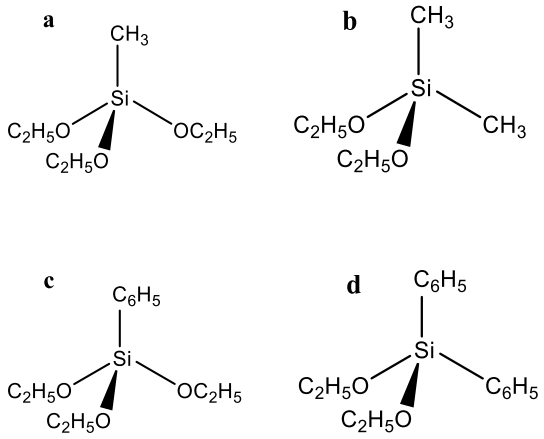

Figure 2: Chemical structures of some common alkoxide precursors used in to synthesize melting gels via the sol-gel process. (a) Methyl triethoxysilane (MTES), (b) Dimethyl diethoxysilane (DMDES), (c) Phenyl triethoxysilane (PhTES), (d) Diphenyl diethoxysilane (DPhDES)

The chemical reactions of hydrolysis and polycondensation that finally lead to consolidation are well characterized in the bulk [19]. These reactions can take place below or above the point of zero charge (PZC) or isoelectric point which lies between pH 1.5 and 4.5 [19, 20]. The PZC depends on the degree of condensation for example the higher degree of condensation the lower the PZC is. When the synthesis occurs below the PZC the OSS is positively charged while when it occurs above the OSS is negatively charged. The nature of the

organic groups also influences the PZC. Condensation under the PZC involves a protonation step of the silanol or alkoxy groups, which has the effect of water or alcohol elimination. Moreover, the protonation of the silanol makes the silicon atoms more electrophilic and susceptible to a nucleophilic attack by water or another silanol. At the pH >3 the reaction advances under the nucleophilic attack of the OH^- or $Si\text{-}O^-$ under a nucleophilic substitution (S_{N^2}) mechanism.

1.1.3 Melting Gels' Useful Properties

The precursors used to prepare hybrid melting gels are both mono- (MTES, PhTES) and di-substituted (DMDES, DPhDES) organo-modified alkoxides as shown in Table 1 and Figure 2. These precursors are mixed at varying mol ratios to produce hybrid gels with varying properties, but the di-substituted siloxane is never present over a 50 mol% in melting gels. Both physical and chemical properties of melting gels arise because of the mol mixing ratios of their reagents. Nuclear magnetic resonance (NMR) has been used to examine the molecular structure of gels with 3D networks, and the resulting spectra have shown 3D siloxane networks with weakly interacting phenyl groups.

Melting gels differ from other classical hybrid gels through their properties. Particularly, melting gels have reversible glass transition points T_g (typically < 0°C) and irreversible consolidation temperatures T_C (typically > 120°C). At room temperature, melting gels have extremely high viscosity and are relatively rigid, but they can be softened by heating to ~70°C for low temperature processing. By sufficiently heating to T_C, a property dependent on composition, silica chains undergo complete cross linking and the melting gel is transformed into a hybrid silica glass which can no longer soften.

1.2 Electrospray Deposition (ESD)

1.2.1 Electrospray Deposition for Micro-Coatings

Electrospraying and the similar technique electrospinning have emerged as a technique to produce micron-scale films since Zeleny first reported electrostatically induced sprays in 1917 [88]. Both techniques apply a high voltage to a solvent medium containing the desired coating particles. Electrospraying typically uses lower solid contents than electrospinning, leading to the propagation of particles via droplets rather than wires.

Mechanisms

Electrospray produces charged, monodisperse droplets of material that are delivered at a continuous rate towards a grounded substrate. As dilute solution exits the stable needle, the interaction of surface tension in the fluid and the strong electric field creates a stable state. This electrostatic spray was first observed and reported by Zeleny in 1917, and the stability was later labeled a Taylor cone, after Sir Geoffrey Taylor demonstrated the disintegration of charged droplets in an electric field due to the pressure difference and charge. The instabilities produced were dependent on droplet size.

$$d = \alpha \left(\frac{Q^3 \varepsilon_0 \rho}{\pi^4 \sigma \gamma}\right)^{\frac{1}{6}} + d_0 \quad \text{[Eq. 1]}$$

$$Q_{min} \approx \frac{\sigma \varepsilon_0 \varepsilon_r}{\rho \gamma} \quad \text{[Eq. 2]}$$

Gañán-Calvo et al. demonstrated that the droplet size in an electrosprayed solution is determined by fluid properties as stated in Eq. 1 [28], where d is the droplet size, α relates to the fluid's dielectric permittivity, Q is the flow rate, ε_0 is the permittivity of vacuum, ρ is fluid density, γ is surface tension, σ is electrical conductivity, ε_r is the dielectric constant.

In electrolytic solutions or ionic liquids, these equations imply the creation of sub-micron (< 100 nm) droplets during electrospray, providing a great advantage in the controlled delivery of small quantities of material. For low conductivity solvents, stability requirements limit electrospray experiments to low flow rates and larger droplet sizes. As a result, lower solid content can be used in low conductivity solvents like ethanol and 2-butanone to compensate for larger droplets while still limiting mass delivery rate. Ultimately, this combination of parameters is useful in order to deliver small quantities during ESD.

1.2.2 Charged Mass Transport Regimes

ESD of Insulating Polymers

The electrospray deposition of insulating polymers on conducting substrates falls into several charge dissipation regimes that are governed by the thermal conditions and, consequently, fluid viscosity and thermal properties. These regimes have ultimately determined the film formation mechanism, affecting final film morphologies as seen in past work [10].

Charged melt sprays operate within a viscous domain, wherein the substrate is at a temperature close to the polymer's glass transition or melting point. The resulting spray is viscous and has low mobility upon arrival at the substrate, hindering its ability to spread and smooth over long distances. As more material is deposited onto the substrate, a film thickening effect is induced, and the trapped charges are unable to adequately dissipate. The extreme growth in film thickness can sometimes trigger fluid instabilities that resemble islands or holes and have been called Taylor-Bénard instabilities due to their resemblance to Marangoni-Bénard convection instabilities.

While charge melt sprays inhibit spray mobility by way of viscosity, electrowetting sprays occur at temperatures above the polymer's glass transition point, resulting in a less viscous spray. As material arrives and accumulates on the substrate, it becomes increasingly difficult for charges to conduct through the insulating polymer to the grounded substrate. To prevent charge accumulation, the mobile fluid spreads laterally, increasing surface area and thinning the resulting film to allow lower resistance to conduction. The net result is a film that spreads like a growing droplet with a thickness that grows nearly linearly with time. Electrowetting sprays, while stable, have been shown to transition into charged melt regimes when a sudden increase in fluid viscosity occurs and charge can no longer adequately dissipate. Lei et al. demonstrated this effect in melting gel sprays during consolidation when the material became more rigid because of cross-linking silica chains[10].

The self-limiting electrospray regime occurs in insulating sprays where polymers arrive on the substrate as a dry spray below their glass transition point. A number of factors influence self-limiting regimes: dry sprays may occur due to the rapid evaporation of solvent, polymers must be hydrophobic to limit interaction with ambient water vapor, and the solvent must be immiscible in water to also limit humidity driven charge dissipation. The self-limiting thickness effect is a result of trapped charges in the deposited polymer as well as in ionized solvent vapor; the charged film repels the similarly charged incoming droplets, preventing the addition of more material after a certain limit. Self-limiting sprays can be optically distinguished from other spray mechanisms because of the cloudy white spray spots generated by light scattering off individual particles.

Electrospray Mass Ionization

The electrospray of conducting materials is more commonly known as electrospray mass ionization due to the charged aerosolization of conducting liquid. It is commonly used in mass spectroscopy as a characterization tool for organic materials. EMI follows a similar mechanism as ESD, where a high voltage is applied to a fluid that causes dielectric break down and separation of smaller charged particles, producing an aerosol or spray jet. Because of the conductive nature of these particles, the aerosol spray consists of droplets orders of magnitude smaller than those in ESD with insulating solvents

1.2.3 ESD of Melting Gels

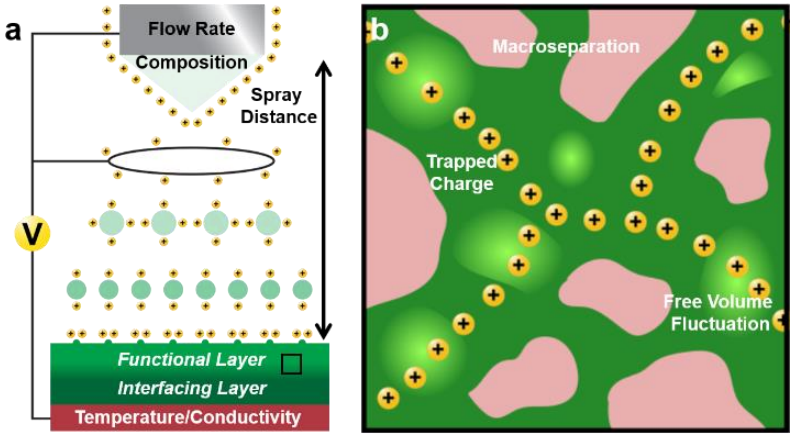

Figure 3: (a) Schematic of the electrospray experimental setup and parameters to be controlled. (b) Schematic of the principal features of interest: trapped charge, free volume fluctuation, and macrophase separation

The electrospray of melting gels presents interesting questions on the effects of charge injection and thermal processing on both the physical morphology of films and the evolution of chemical structure at the molecular level. The chemistry and physics of chemical reactions of highly charged interfaces in both sol-gel and other processes is relatively unstudied, but it is well known that change of the pH of the sol-gel condensation is critical to the dynamics

and the mechanism of reaction. Additionally, ESD's primary advantage of delivering controlled amounts of material is excellent for preparing melting gel coatings, and the added complexity of ongoing chemical reactions during spray further motivates this study. Altering melting gel viscosity by diluting solutions or controlling temperature incorporates the previous aspects of the problem because, as demonstrated by charged mass transport regimes, viscosity greatly affects the ability of a sprayed fluid to spread and dissipate charge, thereby having a significant effect on final film morphology. By dynamically fine-tuning the properties of melting gels via the electrospray process, micro- and nano-scale structures can be controlled to produce final consolidated films with desirable properties applicable to various coating applications.

2. Experimental Section

2.1 Materials

Several melting gels were studied to examine the effects of their composition and preparation conditions on the physical morphology and chemical structure of the final electrosprayed, thermally treated films. Specifically, we examined the interaction of charge injection and consolidation reactions for melting gels prepared with different precursor siloxanes prepared under different pH conditions. Table 2 lists the melting gel compositions used in this study, along with their relevant properties. These melting gels were prepared externally by a collaborator through the sol-gel process. The initial mono-substituted precursor (PhTES, MTES) was mixed in an acidic solution at varying pH levels and stirred for 6 hours at 40°C, after which the di-substituted siloxane group (DPhDES, DMTES) is added and the mixture stirred for 2 hours at 40°C. After the gel forms overnight,

it is dissolved in 2-butanone at 70℃ for 6 hours and thermally treated at 110℃ for 24 hours.

Since the dissipation of charge is linked to the viscosity of the fluid, the decoupling of charge and viscous effects on consolidation is highly challenging. The melting gel synthesis process has been used to tune relevant materials properties. For the purposes of the melting gel, viscosity may be characterized initially by T_g and the molecular weight (Mw) and dynamically by T_c. More specifically, we can model the dynamic viscosity of the MG as a combination of Williams–Landel–Ferry (WLF) dynamics [67] and first-order reaction kinetics as adopted in past studies of thermoset epoxies [68]:

$$\mu(T,t) = C_1 \cdot exp\left(\frac{-C_2(T-T_g)}{C_3+T-T_g}\right) \cdot exp(k(T) \cdot t) \qquad \text{[Eq. 3]}$$

$$k(T) = C_4 \cdot exp\left(\frac{T_c}{T}\right) \qquad \text{[Eq. 4]}$$

Where the C_s are the relevant empirical constants, which contain MW and chemical information about the specific melting gel. Under the assumption that the MW of these oligomeric systems is relatively uniform and that the substrate temperature is far enough above T_g to be in an asymptotic regime of the WLF behavior, we may assume that the largest variations in dynamic viscous behavior will be due to changes in T_c, which is most greatly affected by the chemical composition of the synthesis products of a particular MG. These effects may be seen for the MTES:DMDES MGs previously synthesized in table 2.

TABLE 2: Melting gel compositions and their relevant properties

	Composition (mol %)	pH	T_g (°C)	T_C (°C)
1	87% PhTES, 13% DPhDES	1	25.7	142
2	87% PhTES, 13% DPhDES	1.5	28.54	126
3	87% PhTES, 13% DPhDES	2.5	29.88	135
4	70% MTES, 30% DMDES	2	-6.4	145
5	75% MTES, 25% DMDES	2	-0.3	135
6	65 % MTES, 35% DMDES	2	-18.8	150

The thermal properties of relevant melting gels are shown in table 2. For the purposes of this study, we focused on compositions 1, 2, and 4. Each melting gel has a glass transition temperature around or below room temperature so that each composition results in a rigid film in ambient conditions. Their consolidation temperatures slightly vary, but for these experiments they can all be isothermally treated at 150°C post-electrospray. Table 3 also shows candidate solvents used to deliver material through ESD. As previously described, these low conductivity liquids lead to droplets in the 10 μm range, and so melting gels are diluted to 1 wt% solutions to control delivery rates. Both ethanol and 2-butanone (methyl ethyl ketone) are common solvents used in the electrospray deposition of organic materials because of their compatibility with solutes and their ease of Taylor-cone stability. When not in use, diluted melting gel solutions are sealed in their vials and kept in dry desiccator chambers to avoid contamination.

TABLE 3: Organic solvents used to dilute solutions for small droplet ESD

Solvent	Boiling Point (°C)	Surface Tension (mN/m)	Density (kg/m^3)	Electrical Conductivity (S/m)
2-butanone	80	25	805	2×10^{-5}
Ethanol	78.5	22.39	789	0

Melting gels were electrosprayed onto ~320μm thick, 0.25π in^2 silicon chips obtained by cutting 2" diameter silicon wafers (University Wafer, Inc., N/Ph) into quarters. These substrates were cleaned using standard solvents acetone (Sigma Aldrich) and isopropanol (Sigma Aldrich) to remove dust and impurities. They are then vacuum plasma treated in a Plasma Etch PE-25 plasma cleaning system for 10 minutes to remove unwanted hydrocarbons This treatment is often used in the manufacturing of electronics, medical devices, and plastics, and its ability to fully permeate target substrates improves surface bonding, coating, and wettability. After plasma treating and prior to spraying, these silicon substrates are kept in a vacuum desiccator to maintain surface properties and prolong shelf-life. All melting gel sprays were conducted using dilute solutions of 1 wt% melting gel in as-received high-performance liquid chromatography (HPLC) grade 2-butanone (Sigma Aldrich, > 99.7%). HPLC grade 2-butanone was chosen as the candidate solvent for its high purity and low electrical conductivity.

2.2 Electrospray Setup & Parameters

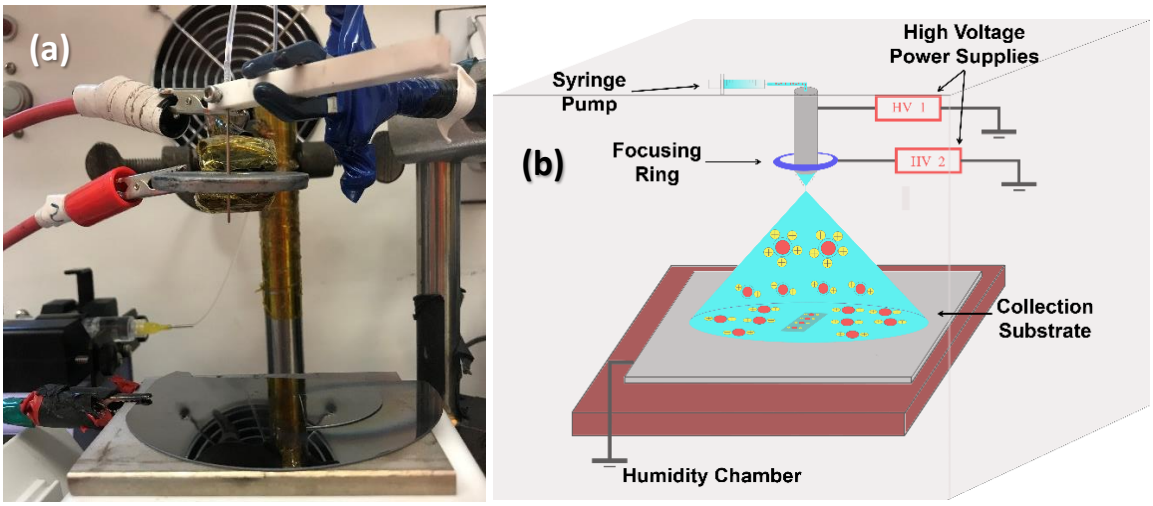

Figure 4: (a) Actual image and (b) schematic diagram of humidity-controlled electrospray setup

The electrospray system consisted of a Harvard, 70-2208 syringe pump, two Acopian, P012HA5M high voltage power supplies (positive sprays), and two Acopian N012HA5M high voltage supplies (negative sprays). A disposable 6-mL syringe (NORM-JECT®) containing the spray solution is fitted into the syringe pump and pumped through PTFE tubing and a stainless-steel needle (SAI Infusion, 20 gauge, 1.5" long) at a constant rate of 0.4 mL/hr. The delivery media are replaced between experiments so as to prevent separation of melting gel from solution as well as to avoid contaminating the spray with dissolved PTFE. The solution is charged at the needle then passed through a weaker radial field produced by a steel focusing ring (2cm inner diameter, 4cm outer diameter, 3mm thick) that provides additional Taylor cone stability. The chips were placed on a large silicon wafer atop a steel block and ceramic hot plate (Fisher Scientific) which were then grounded to prevent charge accumulation. All tests were conducted with the needle tip located 6-cm above the silicon substrate and protruding 1-cm below the charged ring

(Figure 4a). This combination of ESD parameters effectively ensures the absence of solvent upon arrival of child droplets on the substrate. The applied voltages were recorded with a National Instruments DAQ board and controlled on a Labview interface. All tests in this study were conducted at ~ 6.0 – 6.5 kV, while the focusing ring was kept at ~ 3.0 – 3.5 kV. Positive polarity sprays were conducted in a closed chamber (Electro-tech Systems Compact Temperature & Humidity Glove Box) that controlled humidity at 17-21% and ambient temperature at 24℃, while negative sprays were conducted in a downward duct fume hood (equipment) with similar ambient conditions. Maintaining low relative humidity controls the charge dissipation effects due to ambient water. Both the ETS chamber and fume hood setups contained an air flow and filtration system that collected solvent vaporized during electrospray. After spraying, melting gel films are transferred to a ceramic hot plate and isothermally treated at 150℃ for at least 7.5 hours and up to 24 hours.

Melting gels in Table 2 were electrosprayed for 30 minutes at a range of temperatures (150-210 ℃) according to the procedure previously described. This temperature range is well above each composition's glass transition temperature, therefore providing a range at which the melting gel can flow on arrival. Operating above T_C, the consolidation process is also initiated at the substrate during spray to allow for the complex interaction of charge injection, hydrolysis, and polymerization. At each stage, the electrospray continued to produce a stable jet until the desired temperature was attained. Once the system was both thermally and electrostatically stable, the silicon chips were placed in the center of the developing melting gel film. The collection substrate underneath the sample was replaced every hour (in between sprays) to prevent charge accumulation on the surface from

disrupting film formation on the target. To examine the effects of electric field polarity, the same temperature series was conducted under similar conditions while applying a negative potential on the needle and focusing ring.

2.3 Characterization Techniques

Both physical morphology and chemical structure are of interest when characterizing the electrosprayed films. Film uniformity of consolidated melting gel films was measured on a Filmetrics micro-reflectometer by evaluating film thickness, roughness, and optical properties using the properties of silica. Samples were additionally imaged on a Leica optical microscope to provide qualitative data on film characteristics. ATR FT-IR spectra were collected to analyze the final chemical structure on the surface, identifying hydrogen bonding, bonding between solvent and melting gels, and determining whether solvent is fully eliminated from the final hybrid glass coating. To further examine surface properties, water contact angle measurements were taken from optical images from droplets placed in the center of samples.

3. Results

3.1 Choosing the Optimum Spray Solvent

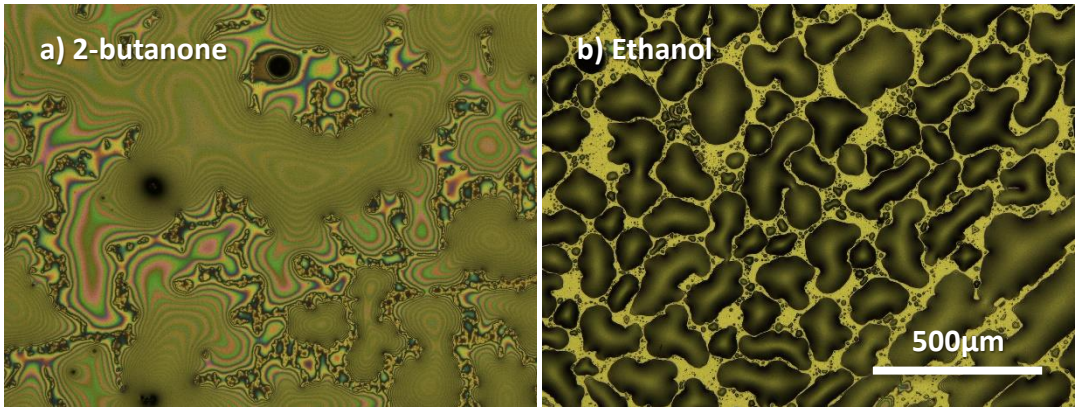

Figure 5: Optical images of 87:13 PhTES:DPhDES melting gel sprayed in a) 2-butanone and b) ethanol at 150°C for 30 minutes at 0.4 mL/hr and positive polarity

To determine a basis for experimental parameters for this study, an initial spray test at positive polarity was conducted for a phenyl-substituted melting gel in different solvents. "Ideal" or "optimal" spray conditions as described in this study are defined empirically according to the desired applications' requirements; they generally refer to electrospray and heat treatment parameters that result in uniform films. Ethanol and 2-butanone were chosen as candidate solvents for their low boiling points and electrical conductivity. Particularly, these properties at this flow rate lead to ESD child droplets on the order of 10 µm according to the droplet and flow rate equations [Eq. 1-2], allowing for the controlled delivery of small quantities of material. The low boiling point ensures that residual solvent is removed with ease. While both sprays resulted in non-uniform films (which will be further discussed), 2-butanone was more successful at coating smoother films. The ethanol spray resulted in large droplet instabilities characteristic of the spray's inability to spread and dissipate charge. These features closely resemble the Taylor-Bénard cells that arise in charged melt sprays. During ESD, the needle and ring voltages were kept at 5.4/291 kV for

ethanol and 6.11/3.24 kV for butanone, but the melting gel sprayed from ethanol was more difficult to stabilize; when conducting ESD experiments, these difficulties were in the form of unstable Taylor cones resulting in the non-uniform delivery of melting gel material. The spray instability in ethanol could have also been a result of melting gel viscosity and particulates if material had not properly dissolved.

3.2 Film Uniformity as a Function of Thermal Conditions

Following the initial solvent test, each melting gel was sprayed in 2-butanone at a series of temperatures as a basis to observe the effects of increasing thermal energy on their ability to spread and dissipate charge as predicted by the charged mass transport models previously outlined. The optical images shown in the following section were taken in the center region of each spray sample where thickness measurements were also taken.

3.2.1 Instabilities in Phenyl Melting Gels

Characterizing Films with Optical Images

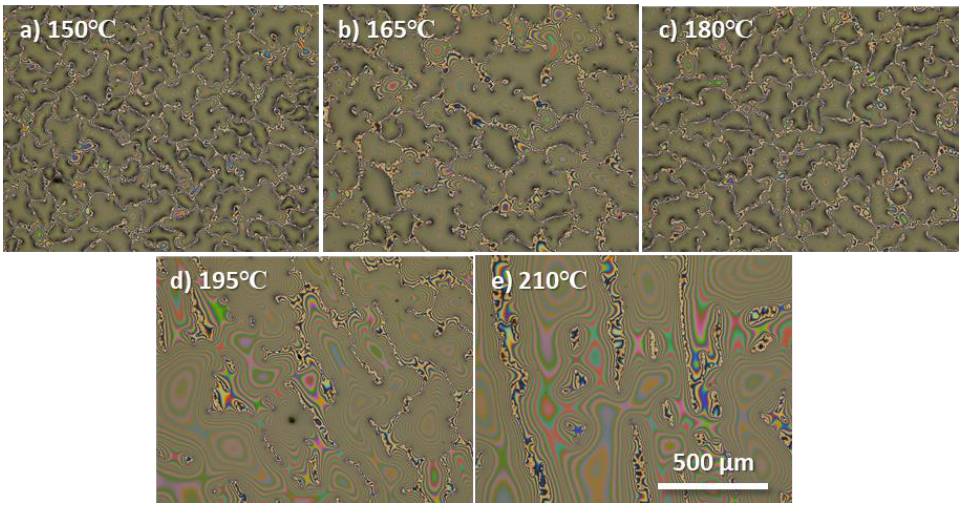

Figure 6: Positively charged sprays of 87:13 PhTES:DPhDES pH 1.5 at increasing temperatures

Optical images provide a qualitative comparison, and consequently help develop an intuition, of different melting gels electrosprayed under the same temperature conditions. The melting gels' tendency to form smooth, uniform films or dewet into condensed structures is evidently dependent on a variety of factors: melting gel composition, substrate temperature, and humidity. Composition and humidity are controlled in each test by using the same melting gel solution and maintaining humidity in a closed chamber. The morphologies achieved at different temperatures suggest a proportionally strong thermal dependence. Figure 6 shows a series of 87:13 PhTES:DPhDES melting gel sprayed at increasing temperatures 150-210℃. At 150℃, the MG is near its consolidation temperature T_C = 126℃, and the spray develops into a non-uniform film with islands of clustered material that resemble large coagulating droplets. These discontinuous clusters thicken at more extreme rates than would a smooth film, as evidenced by their darker edges (an optical effect produced by transparent films with sharp angles). As seen in Figure 6 d-e), increasing the temperature imparts the thermal energy needed to provide some smoothing and is, to a limited extent, able to form a cohesive film. The instabilities at these higher temperatures have flatter, more reflective edges as compared to cells at lower temperatures (as seen in the more colorful reflection patterns) that come in contact with impurities that attached to the surface at some point during the coating process. These particles, likely dust in the air, could indicate that the melting gel would have formed a continuous smooth film if in a cleaner, more controlled environment.

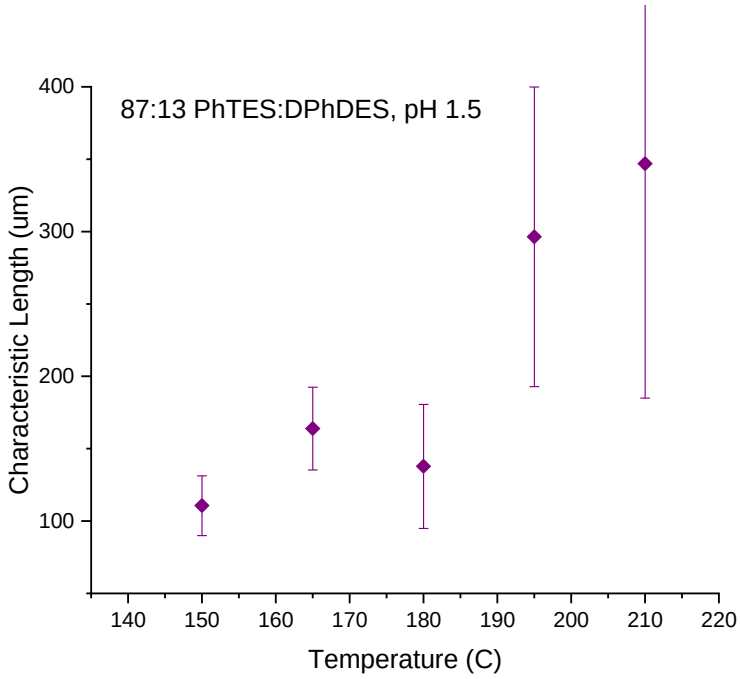

Figure 7: Characteristic width of individual instability cells found in 30-minute negatively sprayed phenyl-based (pH 1.5)

The effect of decreasing viscosity can be observed in the increasing width of individual cells or instabilities. Figure 7 shows the average lengths of individual cells, measured at the narrowest end to end region of each cell. While at the lowest temperature they are narrower, more uniformly distributed, and overall grow thicker at faster rates, at higher temperatures they are wider and flatter with larger variations in size. This flattening signals the electrowetting regime becoming more prominent. It is important to note, however, that Figure 6c) at 185°C shows a regression in instability size that corresponds with the decrease in characteristic length seen in Figure 7. Here, the film diverges from the trend of results and more closely resembles the results obtained at 150°C. This effect is likely due to charge accumulation on the underlying grounded substrate which also builds up incoming spray. As more material deposits that is unable to spread and dissipate charge, incoming spray begins experiencing a repulsive force that alters charge dissipation

mechanisms. As a result, the increased mobility at lower viscosity and higher temperature is offset by the charges trapped in the substrate, and instabilities continue to grow and prevent charge and mass transport. The large standard deviation in cell width seen in figure 6 is a result of the smoothing seen at higher temperatures, where the "characteristic length" that was measured corresponds to the average distance between consecutive dust particles.

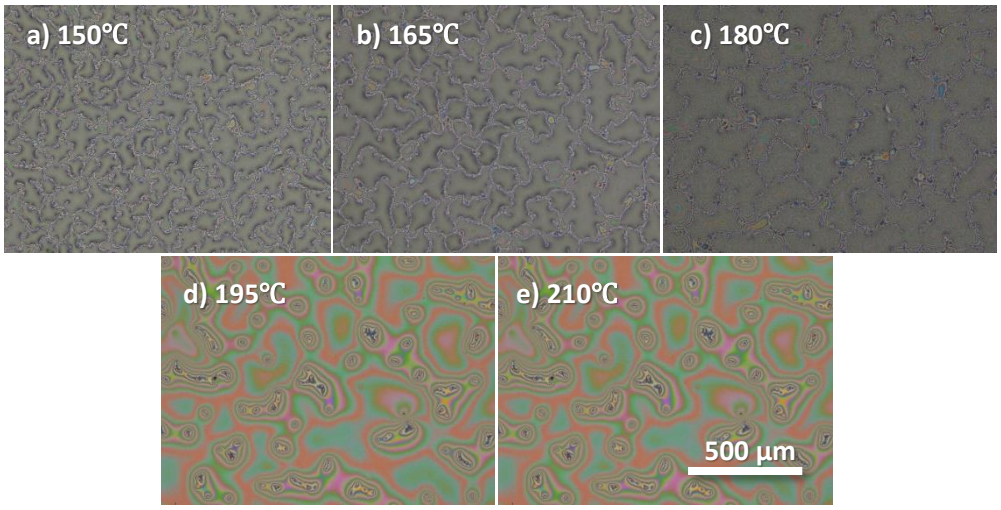

Figure 8: Positively charged sprays of 87:13 PhTES:DPhDES pH 2 at increasing temperatures

Figure 8 shows sprays of the same phenyl-substituted melting gel composition synthesized at a different pH. The same cellular instabilities are observed here, but the effect of temperature and viscosity are more pronounced as seen in the constant decrease in instabilities or increase in uniformity. In figure 8d-e), the higher substrate temperatures successfully smooth the film and eliminate the cellular structure present at lower temperatures. While impurities on the film cause some non-uniformity, the continuous nature of the film signal successful electrowetting and spreading. The reflection patterns off of the optical microscope also indicate relatively uniform film thickness.

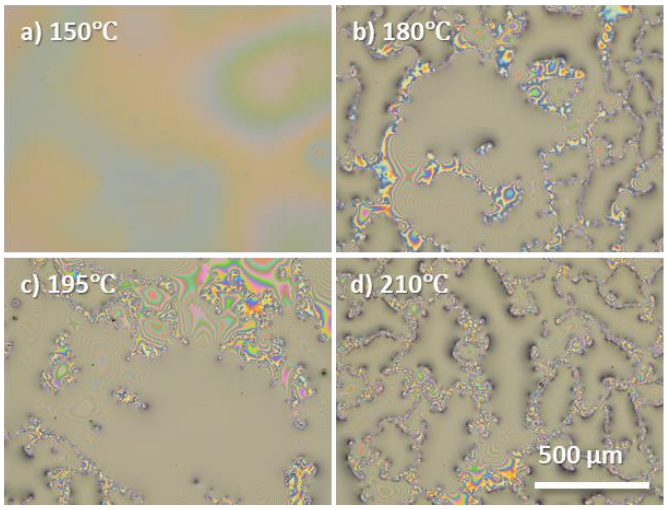

Figure 9: Positively charged sprays of 87:13 PhTES:DPhDES, pH 2.5 at increasing temperatures

It is interesting to note the opposite trend that occurs in Figure 9 for positive sprays conducted at various temperatures for 87:13 PhTES:DPhDES synthesized at pH 2.5. Optical images show that electrospraying around the consolidation temperature $T_C = 135°C$ produces the smoothest film, and further increasing the temperature triggers cellular instabilities. This behavior could indicate that this melting gel composition has a relatively low optimum thermal processing during electrospray deposition. Above these ideal conditions, the extreme temperatures could drastically speed up consolidation, during which melting gel viscosity increases dramatically. As a result, melting gel is no longer mobile on arrival and cannot smooth into a uniform film. If these instabilities are triggered from the onset, then subsequent arriving droplets will continue to dewet.

Dewetting vs. Charged Melt

The smoothing that results from the decrease in viscosity might initially signal the transition between charged melt and electrowetting regimes. In these experiments, viscosity and charge dissipation clearly have an impact on the morphology of the coating.

Cellular instabilities are characteristic of charged melt sprays where material clumps to introduce thinner regions with lower electrical conduction resistance. However, these experiments were all conducted well above the glass transition temperatures of each melting gel, allowing sufficient mobility for the gels to spread over long distances and dissipate charge. Rather than a viscosity effect, we propose that these instabilities arise due to the melting gel films *dewetting* upon arrival at the substrate. The gels' high hydrophobicity and surface adhesion are likely responsible for the films' inability to increase its surface area and smooth. This is supported by the more uniform coatings produced using a methyl-substituted melting gel composition (MTES/DMDES). While exploring higher temperatures may allow for higher quality films, these regimes may begin to decompose the melting gels upon arrival, giving rise to the need for a different mechanism to control film uniformity during ESD.

3.2.2 Electrowetting MGs: Viscosity Driven Spreading

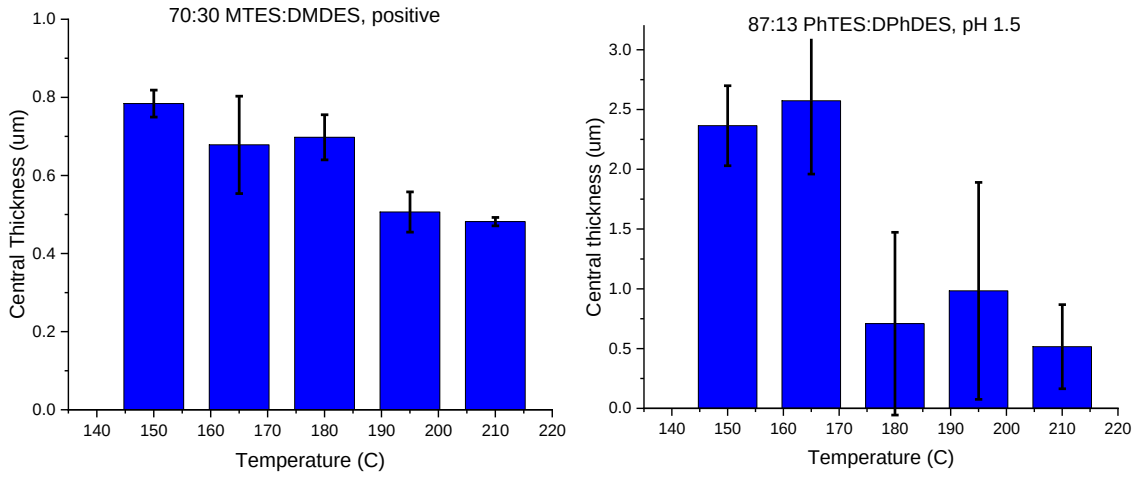

Figure 10: Central thickness of positive 30-minute sprayed (a) (left) 70:30 MTES:DMDES melting gel and (b) (right) 87:13 PhTES:DPhDES pH 1.5 as a function of substrate temperature

Methyl-based melting gels are an excellent candidate to study the effects of viscosity-driven spreading because of their better uniformity. Figure 10a) shows the evolution of film thickness with varying substrate temperature for methyl melting gel sprayed at a positive polarity for 30 minutes. These central thicknesses were measured from the central 1x1 cm^2 spot of the collection substrate. As dictated by the electrowetting phenomenon, increasing the substrate temperature decreases spray viscosity and allows for higher mobility. Consequently, the melting gel spreads laterally, leading to thinner overall films with higher temperatures. There is an evident outlier in the spray conducted at 180℃; rather than following a continuous decrease in thickness, melting gel sprayed at 180℃ increased in thickness for an average central thickness of ~0.69μm. Nevertheless, film thickness has a nearly linear dependence on temperature within this range, decreasing by 5.2 nm/℃ with R^2 ~ 0.888 (if the result at 180℃ is neglected, R^2 ~ 0.971). This linear progression cannot be extrapolated indefinitely, however, as other properties become prominent outside this range; for instance, the increase in viscosity closer to room temperature would greatly impact melting gel mobility and charge dissipation while the increase in temperature beyond 210℃ would begin to decompose the gel's organic groups. Nevertheless, this temperature range provides an approximate range within which this melting gel composition can be sprayed according to desired applications.

Owing to the dewetting occurring in phenyl-based melting gel sprays, the thickness profiles seen in Figure 10b) do not cleanly fit a trend as do the profiles of methyl melting gels. At lower temperatures 150-165℃, the resulting central thicknesses are much larger than at higher temperatures. When compared with the optical images in Figure 6, it is evident that these thickness shifts are due to the extreme growth in dewetted cells; while

the total material delivered remains constant between these samples, dewetting causes the melting gel to build up into convex cells. The sudden decrease coupled with the rise in temperature illustrates higher mobility of the gel that results in the film leveling out and growing laterally.

3.3 Variations in Chemical Structure due to Temperature

Varying substrate temperature during ESD theoretically alters the internal energy of the melting gel, which influences the breakdown and formation of chemical bonds present in the silica network. Depending on relevant bond and activation energies, different thermal treatments could facilitate the hydrolysis and polymerization reactions that occur to permanently cross-link silica chains.

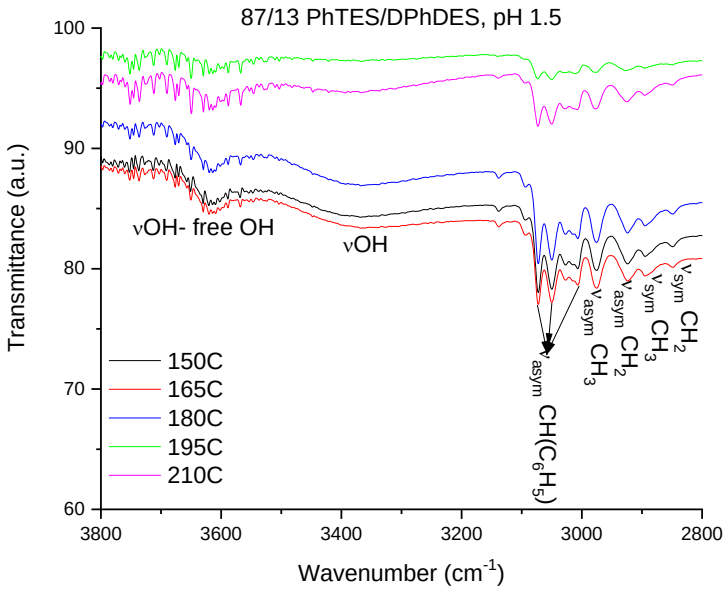

Figure 11: ATR FT-IR spectra for positively sprayed 87:13 PhTES:DPhDES pH 1.5, 30 minutes, at different temperatures

The complete formation of melting gels' 3D network can be characterized by the presence of remaining bonds after charge injection and thermal treatment. Figure 11 shows the resulting spectra for a phenyl-substituted melting gel synthesized at pH 1.5 and sprayed at a positive polarity at various temperatures. At lower temperatures 150-180℃ (black, red, blue traces), the characteristic vibrations at higher wavenumbers >3200 cm^{-1} indicate the presence of underlying hydroxyl and free hydroxyl groups leftover from siloxane precursors. At a delivery distance of 6cm and substrate temperature above the solvent's boiling point (80℃), all remaining solvent should have evaporated during ESD; however, the presence of organic groups at lower wavenumbers suggests the entrapment of organic solvent 2-butanone during ESD and thermal treatment. At higher temperatures 195-210℃ (pink and green traces), these unwanted hydroxyls and alkoxy groups are no longer present, indicating that the optimum temperature at which to electrospray this melting gel composition is around 195℃. This conclusion corresponds with the morphological information seen in Figure 6, where increasing temperature results in smoother and more uniform films.

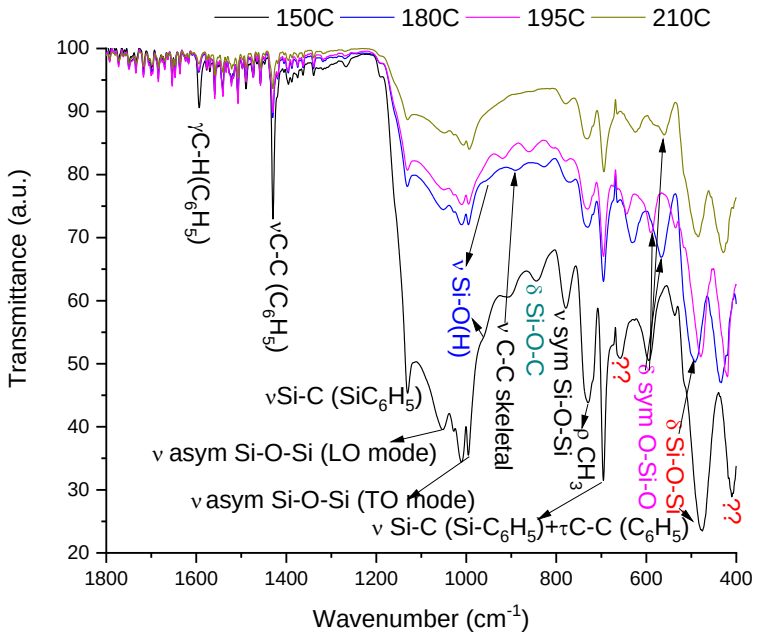

Figure 12: ATR FT-IR spectra for positively sprayed 87:13 PhTES:DPhDES, pH 2.5, 30 minutes, at various temperatures

The pH of melting gel synthesis also factors into the ideal ESD conditions for film preparation. Figure 12 shows FT-IR spectra obtained for a phenyl-based melting gel synthesized at a higher pH 2.5 and sprayed under similar conditions as in Figure 10. Characteristic vibration responses at 900-1000 cm^{-1} in the 150°C (black) and 180°C (blue) traces signal the presence of Si-OH in the melting gel. Organic groups are present in all thermal treatment conditions for this positive spray, suggesting that these groups are somehow protected in this ESD mode and are unable to break down during consolidation. The spray treated at 195°C (pink) had the lowest concentration of transverse Si-O-Si (TO) bonds formed while also showing a shift in alkoxy vibrations; this indicates that the alkoxy groups left over from precursor reagents have begun to decompose at higher temperatures, but they are still present in varying degrees potentially due to a rotation in the bonds. As a result, condensation is inhibited, and a lower number of Si-O-Si bonds are formed. These

spectra suggest that the optimal ESD temperature for this composition in the positive mode is 210℃ (gray), where all alkoxy groups are eliminated and the net result is a dense film with remaining phenyl groups found only on the surface.

3.4 Polarity Effects: Morphology & Chemical Structure

3.4.1 Formation of 3D Network

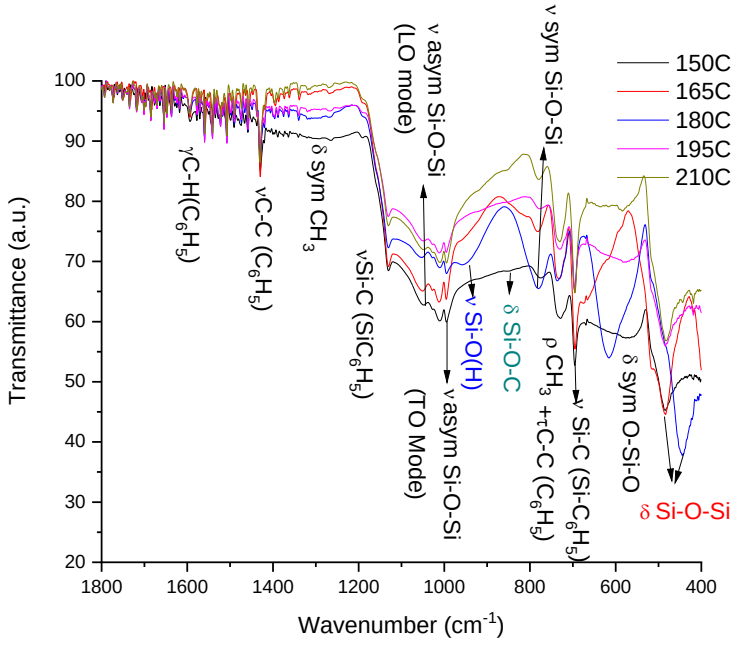

Figure 13: ATR FT-IR Spectra of 87:13 PhTES:DPhDES, pH 2.5, 30 minutes, negative polarity, at various temperatures

The effects of charge injection are evident in the difference in chemical structure observed in melting gel sprayed under similar thermal conditions at different polarities. Within the same polarity mode, thermal treatment still plays a role in the simultaneous consolidation reactions. FT-IR spectra of a negatively sprayed temperature series of phenyl-substituted melting gel shows clear temperature differences within the same polarity as well as external differences when compared to positive sprays of the same

composition and pH. The characteristic vibration for the presence of remaining ethoxy groups Si-O-C is present for samples sprayed at 150°C and 165°C (black and red traces respectively). These ethoxy groups disappear at higher temperatures, likely due to condensation or elimination induced by thermal treatment. As seen in the 1200 cm^{-1} peaks, Si-C(C_6H_5) bonds are independent of thermal treatment as they are still present for all samples in this temperature range, indicating that they are not affected by the hydrolysis and polycondensation reactions that occur during consolidation. The stretching of Si-O-Si structures in the transverse mode are also present and can be compared to the stretching of the Si-C bonds; the asymmetric stretching of the former is an indication of the formation of the 3D network. According to the spectra obtained here, the optimum substrate temperature at which to spray this melting gel composition at a negative polarity is 165°C or 210°C. The presence of symmetric Si-O-Si structures is an interesting result that needs further investigation.

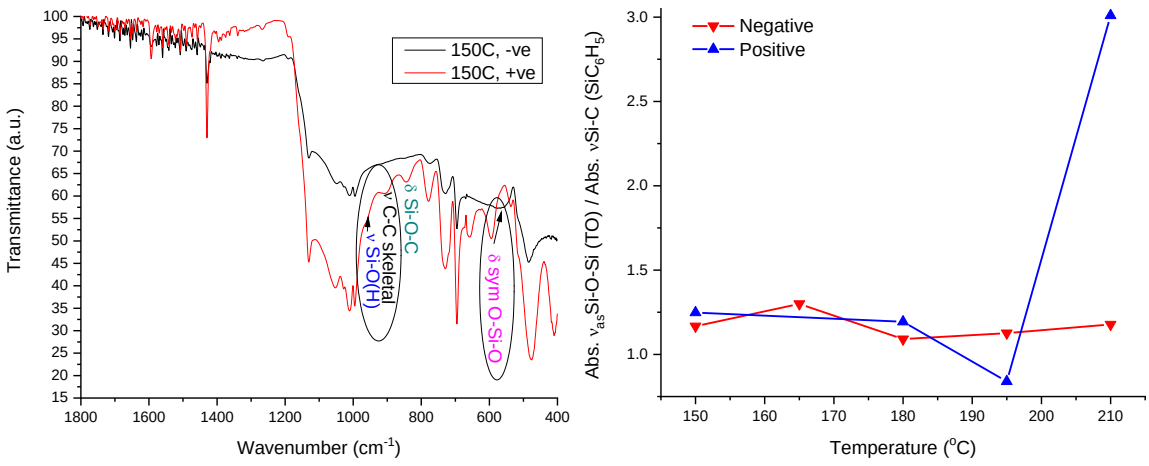

Figure 14: a) (left) ATR FT-IR of 150°C, 30 minute sprays of 87:13 PhTES:DPhDES, pH 2.5, (b) (right) A polarity comparison of the ratio of transverse Si-O-Si to Si-C(SiC_6H_5) bonds as it varies with substrate temperature

The effects of polarity can be better inspected by contrasting samples sprayed under similar conditions at different polarities. Figure 14a) shows phenyl-substituted melting gel (pH 2.5) sprayed near consolidation temperature at 150℃ for 30 minutes at both positive and negative polarities. Isolating polarity effects from temperature effects allows a clearer comparison of the effect of charge injection for different electrospray modes. Vibrations at ~ 1000cm^{-1} in the positive (red) trace show the presence of silanol Si-O(H) that is not found in the negative (black) spray, while the peak at ~850 cm^{-1} indicates the presence of Si-O-C that did not hydrolyze during the consolidation process. For the same thermal conditions, injecting melting gel with negative charge better enables the breakdown of unwanted structures during hydrolysis and consequently allows better formation of the hybrid gel 3D network.

The ratios between ν OH and ν_{as} Si-O-Si (TO) and also between ν_{as} CH_3 and ν_{as} Si-O-Si (TO) indicate the extent of consolidation and the degree of degradation of the organic groups and which reactions are dominant. The presence of Si-C(SiC_6H_5) can be used as a standard against which to evaluate the effectiveness of thermal treatment and charge polarity on the formation of melting gels' 3D network. Figure 14b) shows the concentration of transverse Si-O-Si structures remaining in the consolidated melting gel relative to the concentration of Si-C(SiC_6H_5). The graph shows that their ratios in oppositely charged sprays remain relatively constant for lower temperatures, fluctuating around 1.25. Increasing substrate temperature to 195℃, however, shows a sudden decrease in transverse Si-O-Si levels with respect to Si-C(SiC_6H_5), dipping to ~ 0.2. Further increasing thermal treatment temperature in the positive spray then results in a dramatic increase in Si-O-Si as seen at 210℃.

3.4.2 Film Morphology

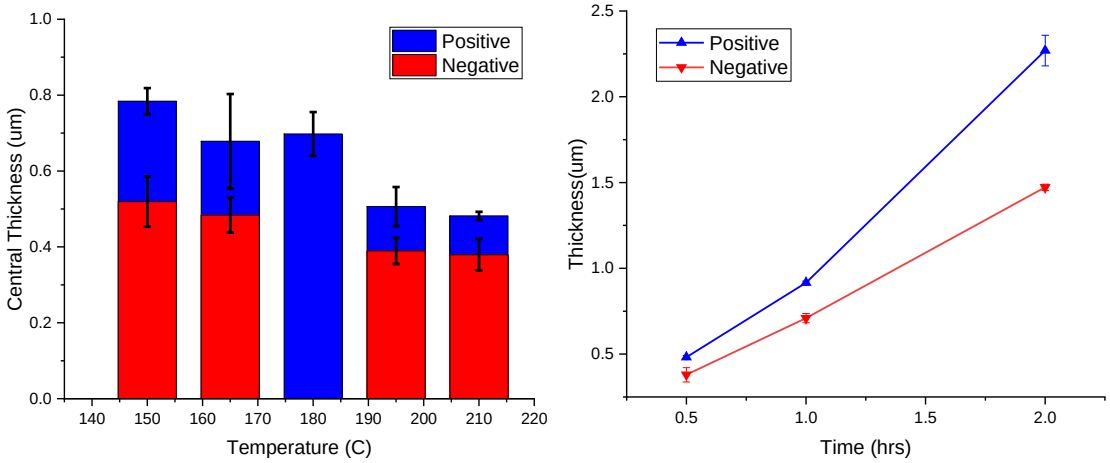

Figure 15: Thickness comparison for 70:30 MTES:DMDES, pH 2 melting gel sprayed at different polarities: a) (left) temperature series for constant mass, 30 minute sprays, b) (right) isothermal sprays with increasing total mass

To investigate the effects of charge injection on morphology, methyl-substituted melting gel was sprayed at different temperatures (Figure 15a) and for different times (Figure 15b). The methyl-based melting gel was the most suitable composition for characterizing physical properties because its lower surface adhesion allowed for more uniform coatings. Each polarity fits within the electrowetting model, demonstrating that increasing substrate temperature during ESD decreases viscosity and leads to lower overall thickness. However, negatively charged sprays produce a much thinner film, with an average difference of ~0.205 μm. This thickness difference is largest at the most viscous spray conducted at 150°C, where the positively sprayed film attains a final thickness of 0.784 μm and the negative only reaches 0.38 μm. The effect of temperature is also less prominent in negatively charged sprays, where a linear curve fit shows that film thickness decreases at approximately 2.4 nm/°C (R^2 ~ 0.9407), as compared to the 5.2 nm/°C previously observed in positive sprays.

As seen in Figure 15b), both positively and negatively sprayed films grow almost linearly with time, but the former shows a more rapid growth rate. Overall, negatively sprayed films always result in a lower final thickness, owing to the greater dissipation of charge across the surface or the higher spreading rate thinning the film. The linear growth is significant because it confirms that these sprays operate within the electrowetting regime, where viscosity and charge dissipation dictate the thickness and with of sprayed films. The morphological difference resulting from these electrospray modes is likely a result of a difference in charge trapping mechanism; droplets are able to better trap negative charges during electrospray, causing greater charge dissipation in the electrowetting transport regime.

3.5 Mechanical Properties

Coatings used to protect against corrosion and other wear must be mechanically robust to provide adequate shielding for underlying components. To characterize important mechanical properties of electrosprayed melting gels, methyl-substituted melting gel was sprayed at 210℃ for 2 hours at a positive and negative potential and then tested with a nano-indenter. These sprays resulted in a final thickness of 2.27 μm and 1.47 μm respectively (as seen in Figure 15b). As when studying film morphology, the uniformity of methyl films is desirable when characterizing mechanical properties that arise from charge injection.

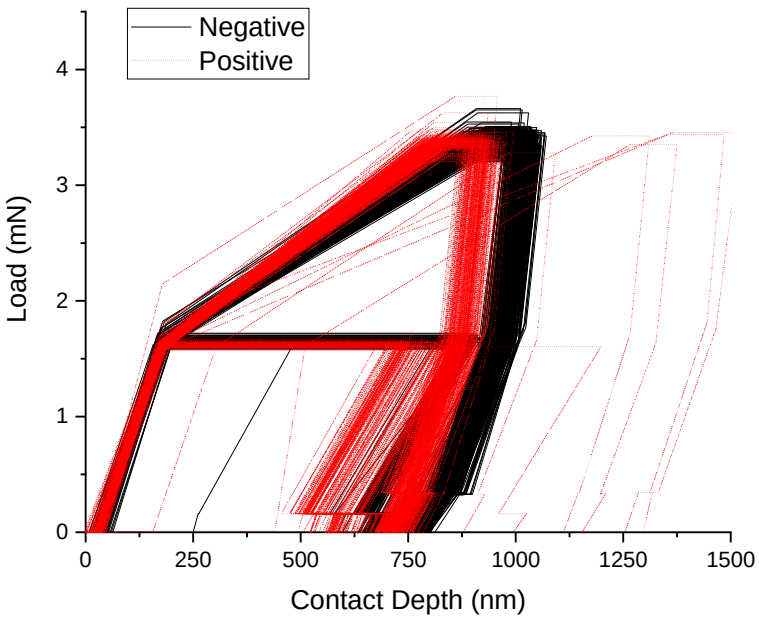

Figure 16: Loading and unloading profiles for 2hr positively and negatively charged 70:30 MTES:DMDES sprays at 210℃

Nano-indentation tests were performed on the methyl melting gels in a depth-controlled mode, using a constant loading and unloading rate. The hysteresis curve for each test is shown in Figure 16. Indents on the positively sprayed sample applied a maximum load of 2.814 mN while the negative had a maximum of 2.770 mN. The general loading and unloading profiles are similar for each sample, showing similar deformation rates and load levels for the same contact depths. A shift in the load-depth curve occurs at ~1.6 mN and ~160 nm for both the positively and negatively sprayed melting gels, signifying a shift in elasticity and hardness of the sprayed samples. This apparent dependence on contact depth suggests another effect of charge injection on the consolidation process; while thermal treatment occurs over a much longer period of time (up to a total of 24 hours) than does the electrospraying process, the gel's mechanical properties do not normalize

throughout the film. Consequently, there is no single value of hardness and elasticity that can reasonably be calculated for the bulk.

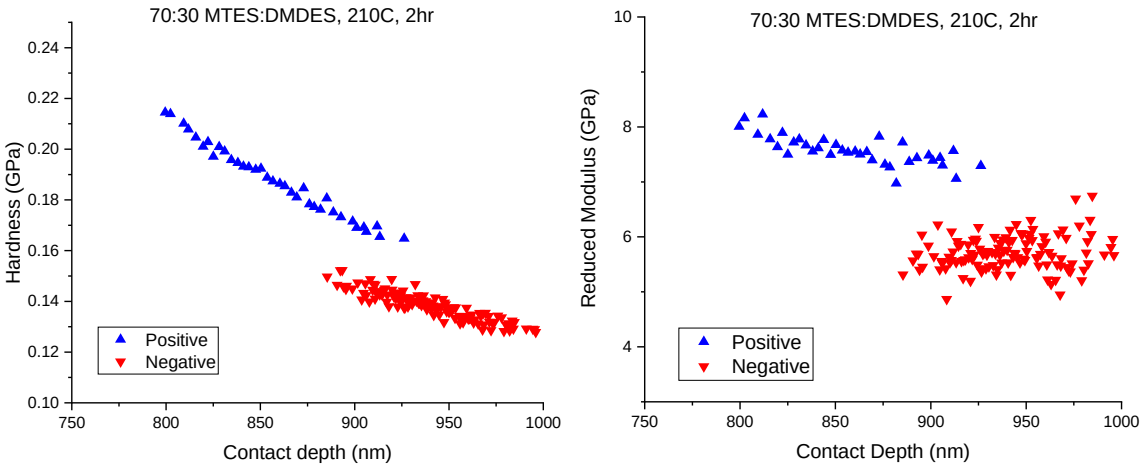

Figure 17: Mechanical properties at individual indents from depth-controlled nano-indentation tests on methyl-based melting gel sprayed at 210°C for 2 hours: (a) Hardness vs. Contact Depth, (b) Reduced Modulus vs. Contact Depth

To better examine the consolidated melting gels' mechanical properties, their local hardness and reduced moduli can be plotted for individual loads. The values shown in Figure 17 were fitted according to the methodology previously described in the Experiment section using measurements at 10-100% of unloading data. Both polarities have a downward trend in material hardness with increasing contact depth, with the positively charged sample having a higher overall hardness. This difference may be partially attributed to the thickness difference seen in Figure 15b), with the thicker positive sample suggesting a high bulk hardness, but the influence of charge injection and polarity still need further study. The elasticity of each sample can also be quantified by studying the reduced modulus which accounts for deformations in the Berkovich tip. A similar trend is seen in Figure 17b) where the modulus decreases with increasing load albeit at a slower rate. Local

differences in moduli are greater here, seen graphically in the plot's sparser distribution. This disparity is even more pronounced in the negative melting gel. As seen in Figure 11a), polarity has a distinctive effect on the chemical structure of 87:13 phenyl-based melting gel sprayed at 150℃, so in addition to causing greater charge dissipation, negative sprays can also affect other film properties. While FT-IR spectra are not currently available for this composition and these ESD parameters, we can safely assume that polarity influences the chemical structure, and hence the mechanical properties, of the final melting gel film.

3.6 Surface Properties: Hydrophobicity

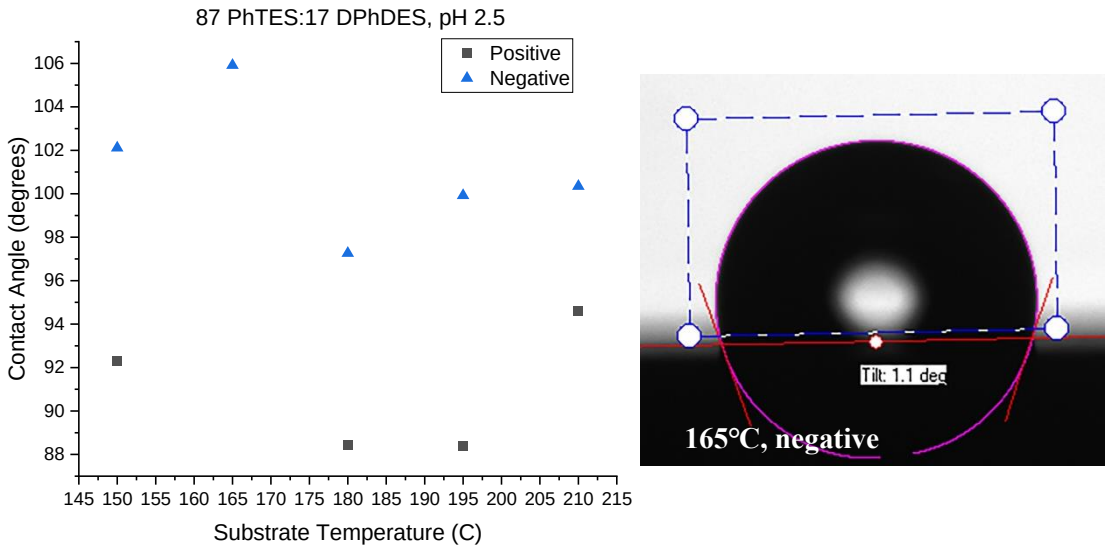

Figure 18: (a) (left) Contact angles measured on 30-minute sprays of 87:13 PhTES:DPhDES pH 2.5, (b) (right) Optical image of water droplet on the surface of phenyl melting gel negatively sprayed at 165℃

Interaction with water and water vapor is an important feature to examine in coatings. Hydrophobicity and hydrophilicity levels provide information on coatings' surface properties, most importantly surface tension. Figure 18 shows water contact angle

measurements taken in the middle section of 87:13 PhTES:DPhDES, pH 2.5 sprays. In general, consolidated melting gel films are hydrophobic. Melting gel sprayed at a negative polarity results in higher hydrophobicity with contact angles above 97°, while those sprayed at positive polarity are less hydrophobic with angles below 95°. These measurements indicate that the ideal negative polarity ESD temperature for this composition is 165℃ where it is most hydrophobic with an angle of 106°. This general trend and optimal condition are in excellent agreement with the FT-IR spectra obtained for the same sample. The interaction with water droplets, or the lack thereof, is indicative of the absence of polar organic groups that would have been present in the pre-consolidated melting gels; the breakdown of these bonds signals the complete formation of the hybrid silica network through hydrolysis and polycondensation. It is important to note that due to the dewetting and non-uniformity in these phenyl-substituted melting gels, the hydrophobicity of samples is partially due to the microscale texture and the hydrophobic silicon substrate. These results need to be reproduced on smooth films and compared with bare silicon wafers and spin-coated melting gels (to eliminate charge injection effects). However, we can expect that the agreement in surface properties as illustrated by both FT-IR spectra and goniometry still provide meaningful results.

4. Discussion

4.1 Film Morphology

Film smoothness and uniformity are necessary qualities to produce high quality coatings in any field. Although the sol-gel process successfully produces non-porous,

crack-free melting gels, non-uniformity in electrospray deposition would compromise the integrity of coatings, providing inadequate anti-corrosive protection in metals and improper sealing in electronic components. The dewetting instabilities largely present in phenyl-based sprays are a clear obstacle to overcome. As seen in the general progression of melting gel coatings at increasing temperatures, decreasing viscosity by increasing thermal energy partially succeeds at counteracting surface adhesion in the melting gels and allows films to thin and smooth over longer distances. While further increasing the temperature may allow for greater uniformity, there exists a limit at which new challenges may arise; in particular, organic groups within the gel solution may start to decompose. Consequently, this would interrupt the hydrolysis and polymerization reactions and fail to produce the necessary network in consolidated melting gels. Dewetting can be overcome through other approaches; for instance, surface adhesion can be lowered by testing different surfactant blends. Furthermore, if particulates are the real source of non-uniformity at higher temperatures, these experiments need to be repeated in more controlled environments to verify the optimal electrospray parameters for each composition.

Choosing the right candidate solvent to carry dilute melting gels is important as it determines electrospray flow rate, field strength, stability, material delivery rate, and shelf-life. Melting gels can be synthesized using ethanol or butanone, so it is preferable to use the same organic solvent when diluting solutions for spray to avoid (other remaining solvents disrupting spray stability). Initial sprays of phenyl-substituted melting gel showed a comparison between ethanol and butanone systems; the more uniform coating produced by the latter proved it more suitable for these electrospray setups. However, butanone is a stronger organic solvent than ethanol, and is more likely to dissolve other components in

the spray setup (e.g. the disposable syringe and PTFE tubing) if not replaced frequently. Dissolving unwanted components could introduce solid particles into the melting gel solution, increasing the viscosity and preventing charge dissipation in the spray. The use of butanone also requires frequent replacement of filtration systems; for instance, within our closed humidity-controlled chamber, inadequate filtration would cause an accumulation of vaporized solvent, disturbing charge dissipation and evaporation on the collection substrate. Ethanol would have been a better alternative to account for these shortcomings; however, the largely unstable sprays produced would not be suitable for these coatings. The droplet-like structures seen in the ethanol spray in figure 5 largely resemble a charged melt spray. It is difficult to optically distinguish charged melt spray from dewetting in this result. If ethanol does cause inadequate charge dissipation in this way, it is potentially indicative of improperly dissolved solids; perhaps over time, the melting gel aged and increased in viscosity.

4.2 Melting Gels' Responsiveness to Injection of Negative Charge

Large differences in physical morphology and consolidation arise when varying electrospray polarity modes. Negatively electrosprayed melting gels produce a thinner coating with different chemical structure compared to their positively sprayed counterpart while also showing a lower responsiveness to temperature changes (Figure 15a). Past work comparing positive and negative ion modes in electrospray mass ionization mass spectrometry (ESI-MS) of small organic molecules provides an explanation into the

charging mechanism of droplets. In ESI-MS, ionization of analytes occurs through 3 possible modes [86]:

1. Reduction-oxidation reactions that occur during electrospray
2. Acid-base reactions within electrospray droplets
3. Proton transfer between ions escaping from electrospray droplets in the gaseous phase

Consequently, the acidity (K_a and pK_a) and polarity of the analyte influences its responsiveness to positive- and negative-ion mode ESI-MS. Acidic analytes favor negative mode electrosprays because of their tendency to form negatively charged anions; basic analytes tend to be protonated to form positive cations and thus favor positive mode electrosprays. The well-known interaction of acidic analytes in water is shown below in Eq. 3. Analytes with higher K_a values, or in other worse analytes that are more acidic, have an equilibrium that favors the deprotonated state on the right. The nature of the analyte solvent also influences ESI-MS characteristics: particularly, organic solvents such as the ones used in this electrospray setup tend to shift this reaction equilibrium to the left. During the electrospray process, however, solvent slowly evaporates out of droplets as they move away from the initial Taylor cone, causing a change in size and consequent changes in analyte concentration and droplet pKa. Therefore, it is difficult to exactly predict the responsiveness of analyte-solvent systems based on pKa, but it still provides a basis of comparison for electrospray modes.

$$HA + H_2O \leftrightarrow A^- + H_3O^+ \qquad K_a = \frac{[H_3O^+][A^-]}{[HA]} \quad \text{[Eq. 5]}$$

Because melting gels are synthesized in highly acidic environments ($1 < pH < 2.5$ in this study), this model predicts that they would tend to favor negative electrosprays. The higher

concentration of anions in the solution results in trapping more charges than their positive counterparts, causing greater charge dissipation at the grounded surface. This theory is supported by the morphological evidence seen in methyl-substituted melting gels sprayed at positive and negative polarities. Because there is a greater charge content per droplet, melting gel must dissipate more charge on arrival, spreading on the surface and finally producing thinner films for the same thermal conditions in the positive.

4.3 Improvements to the Experimental Setup

The results obtained in these experiments largely indicate the importance of charge injection on the overall physical and chemical properties of melting gel films prepared via electrospray deposition. There are still variables in the experimental setup that can be better controlled to mitigate unwanted environmental effects. Particularly, unwanted trapped particles in films, like those observed in high temperature phenyl-substituted melting gel sprays, must be eliminated in order to obtain more conclusive information. The positive and negative electrospray systems are also carried out in separate chambers; while ambient conditions such as temperature and relative humidity are controlled, the air flow in these setups is not controlled. Fan blowing in the ETS chamber and downward suction in the fume hood can potentially affect the spreading of the growing melting gel film on the collection substrate and influence film growth. This effect can be mitigated by conducting both spray modes within the same chamber. It is also necessary to observe the consolidation process of melting gels under the same thermal processing conditions without injecting charge through electrospray deposition. Preparing films this way would provide a basis or standard against which to specifically isolate the effects charge injection. Finally, charge accumulation still remains a phenomenon that could distort data by

interfering with charged mass transport mechanisms; in future tests, the grounded collection substrate must be cleaned and replaced with each new sample.

4.4 Applications

By preparing melting gel films through electrospray deposition, there now exists multiple modes of control by which to select useful mechanical, thermal, and optical properties. The mol ratio of precursors used in the sol-gel preparation determine melting gels' thermal properties, which in turn influence ideal electrospray deposition conditions. Because charge injection affects morphology, hardness, and elasticity, electrospray parameters can be controlled to produce highly adhesive melting gel coatings with the desired properties as needed by specific applications.

5. Summary

Melting gels are a class of hybrid organic-inorganic silica gels synthesized via the sol-gel process. They largely differ from other hybrid gels because their mono- and di-substituted siloxane precursors do not undergo hydrolysis during sol-gel synthesis, leading to the incomplete formation of the silica network. These free structures lend melting gels their useful thermoplastic properties, flowing and reflowing above their glass transition temperatures and permanently cross linking with sufficient thermal treatment at their consolidation temperatures. Their low permeability, dielectric properties, and low temperature processing have proven them useful as candidate materials for sealing glasses and anti-corrosion coatings.

Electrospray deposition has been an established technique to prepare micro coatings. Using low conductivity solvents as the medium in which to deliver polymers has allowed for the controlled delivery of small quantities of material, owing to the low solid contents of solutions and the charged, monodisperse droplets induced by high voltages. The complex interaction between charges and chemical reactions during ESD and melting gel consolidation presents an interesting research problem to be explored, as these reactions will impact the final characteristics of melting gel films.

This parametric study of electrospray deposition parameters aimed to investigate the effects of charge injection on the final properties of consolidated melting gels. By varying substrate temperature and ESD polarity, we demonstrated the extensive impact of viscosity and charge injection on the transport mechanisms of fluid melting gels as well on the hydrolysis and polymerization reactions during consolidation. It was found that phenyl-substituted melting gels synthesized at different acidity levels had high surface adhesion and hydrophobicity, hence they tended to dewet into unstable cells that were analogous to Taylor-Bénard cells in the charged melt electrospray regime. Increasing substrate temperature decreased viscosity in these sprays, allowing for greater mobility and smoothing in the electrosprayed films. Overall, this increase in internal energy was able to counteract surface forces in the melting gel to create a uniform film despite dust and impurities. Substrate temperature also had a large impact on the consolidation process: the presence of precursor organic and inorganic groups in samples treated at different temperatures indicated that consolidation was also dependent on thermal treatment despite all samples being isothermally treated at 150℃ post-spray. The net result of these findings

is a set of thermal conditions that are optimal for the electrospray deposition of each melting gel composition as dictated by FT-IR spectra.

Charge injection has an undeniable impact on reactions occurring during consolidation. Negatively charged sprays overall result in thinner films for all thermal treatments when compared to positively charged sprays; depth-controlled nano-indentation on thick methyl-substituted melting gel films reveal that positively sprayed films are 38.22% harder and 3.71% more elastic than negatively sprayed films; examining the FT-IR spectra of consolidated melting gels also illustrates that a different set of optimal thermal conditions exists for each electrospray polarity mode contact angle measurements on phenyl-substituted melting gels illustrate that negatively sprayed films result in higher hydrophobicity overall. These disparities in film morphology, mechanical properties, chemical structure, and surface properties are all a direct consequence of the varying responsiveness of melting gels to positive and negative charges. Melting gels are synthesized in acidic media, making them favor deprotonation in the spray solvent. Consequently, they have a greater affinity for negative mode electrospray. This greater charge trapping results in greater charge dissipation, producing thinner electrowetting films while also impacting the rate of hydrolysis and polycondensation reactions during consolidation.

6. Future Directions

There still exists a vast parameter space to explore that can potentially affect the consolidation process during electrospray deposition. Charge injection evidently causes major changes in the simultaneous chemical reactions that occur during spray, as seen in

final morphology and FT-IR spectra. It is necessary to obtain a basis against which to compare these effects and eliminate any external effects. To provide a control dataset, we propose preparing melting gel films of each composition via spin coating. These films can be coated according to the spin coating variables (speed, acceleration, duration, concentration) that will produce similar thicknesses; to reproduce the thermal treatment during electrospray deposition, they can be heated at the corresponding temperatures for 30 minutes then transferred to 150°C to complete consolidation overnight (~17 hours). The effects of charge injection on melting gel consolidation can then be studied by inspecting the final chemical structure via FT-IR spectroscopy.

Other melting gel compositions still need to be explored. Because each composition results in a different set of thermal and mechanical properties, their electrospray deposition process must be optimized in order to leverage useful properties towards different applications. Varying thermal treatment was used in this study to alter viscosity, but this fluid property can also be studied by using different melting gel blends. For instance, viscosity modifiers such as α-terpineol and dodecane are ultimately expelled from the final film; their presence in the spray solution would be to purely decrease spray viscosity. Melting gel coatings can also be functionalized by adding nanoparticles like silica and zinc oxide; the addition of these solids increase viscosity and, in the case of zinc oxide, increase the conductivity of the spray solution. These compositional studies of melting gels add a level of complexity to the experimental model. As such, the preliminary results found in this initial study provide a useful basis for optimal ESD conditions. For instance, in denser composite sprays, we can take advantage of low temperature processing at negative polarity to slow the consolidation rate allow easier manipulation of charge and viscosity.

The formation of the 3D silica network can be slowed, and the effects of charge injection further observed by reducing the rate of delivery of melting gel. This can be achieved by reducing electrospray flow rates while increasing total spray time, effectively delivering the same overall mass. Individual child droplets in this setup would be much smaller as dictated by the flow rate equation (Eq. 2), resulting in a much higher charge content per mass. In this setup, the films can more quickly consolidate on arrival. According to the electrowetting transport mechanism, the higher charge content would cause greater dissipation and spreading, potentially leading to thinner and wider spray spots. The faster consolidation rates and denser solid concentration per droplet could also trigger a transition from the electrowetting to charged melt regime, where the film forms Taylor-Bénard cells to generate thinner regions through which charges can dissipate more easily.

Past work in the electrospray deposition of insulating polymers has demonstrated its ability to produce thickness-limited films. This phenomenon has had important consequences leading to the coating of complex 3D geometries owing to the spray's ability to wrap around structures and find uncoated regions. The charged nature of electrosprays also presents advantages in the directed deposition and growth of material; it has been shown that focused laser spike (FLaSk) dewetting of thin films can be used to create stencils on insulating polymers that act as templates to direct electrospray. This selective patterning is a consequence of FLaSk dewetting's dependence on molecular weight [87]; by controlling laser parameters like power and spot size, which ultimately determines lateral thermal gradients, softer films can be independently flowed without damaging underlying layers. Templating ESD via FLaSk dewetting would aim to further study the

limits of these complex geometries by transitioning to a control 2D pattern for study. The ability to consolidate melting gels makes them interesting candidates for these targeted sprays, providing an avenue towards potential 3D structures. In particular, their final optical, mechanical, and electrical properties make them useful candidates as silica waveguides or dielectric coatings in flexible electronics.

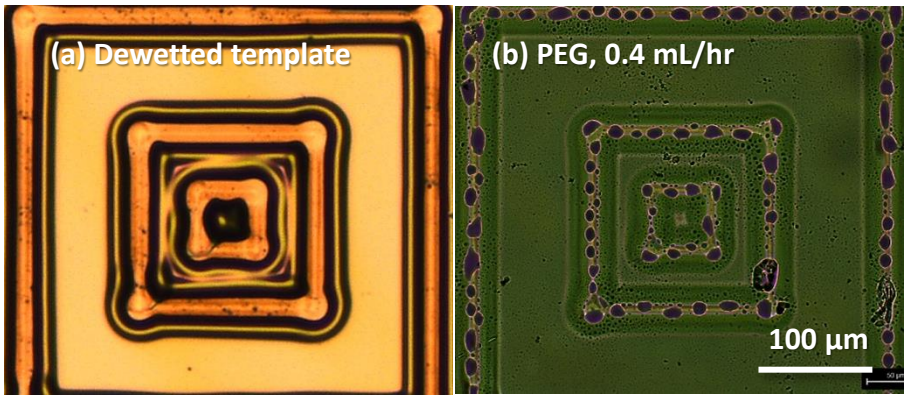

Figure 19: Directed electrospray deposition of dyed PEG onto pre-charged polystyrene-gold films, (a) Dewetted polystyrene on gold, (b) Dyed PEG sprayed into exposed gold regions

To further investigate charge dissipation mechanisms and their implications on melting gel consolidation and morphology, the experimental setup can be altered such that the collection substrate is charged rather than grounded. The substrate can be maintained at a series of voltage levels for both positive (up-bias) and negative (down-bias) polarities. The resulting field will be influenced by the voltages at the needle, focusing ring, and substrate, as well as the relative distances between each component. Up-biasing a positively charged spray, or similarly down-biasing negative spray, is likely to induce some repulsive effect that varies with field strength, potentially causing larger lateral spreading or generating electrohydrodynamic instabilities. Preliminary work in applying a bias

voltage to electrospray substrates has already produced interesting results to explore. Figure 19a) shows a FLaSk-patterned polystyrene on gold film that was sprayed with pure ethanol at a positive polarity, trapping charges in the insulating polymer film. It was then sprayed with dyed poly(ethylene)glycol at the same polarity (Figure 19b). The insulating polystyrene film directed spray into the exposed gold regions, but the trapped charges also produced periodic droplet instabilities within the sprayed film.

7. References

1. Sanchez, C.; Ribot, F.; Lebeau, B. *Journal of Materials Chemistry* **1999,** 9, (1), 35-44.
2. Aparicio, M.; Jitianu, A.; Rodriguez, G.; Degnah, A.; Al-Marzoki, K.; Mosa, J.; Klein, L. C. *Electrochimica Acta* **2016,** 202, 325-332.
3. Klein, L. C.; Degnah, A.; Al-Marzoki, K.; Rodriguez, G.; Jitianu, A.; Mosa, J.; Aparicio, M., Electrochemical Properties of Melting Gel Coatings. In *Advances in Materials Science for Environmental and Energy Technologies V*, John Wiley & Sons, Inc.: 2016; pp 233-241.
4. Aparicio, M.; Mosa, J.; Rodriguez, G.; Guzman, J.; Picard, Q.; Klein, L. C.; Jitianu, A.; *ACS Applied Materials & Interfaces* **2019**, 11, (3), 3493-3505
5. Lien, S.; Wuu, D.; Yeh, W.; Liu, J.; *Solar Energy Materials and Solar Cells* **2006**, 90, (16), 2710-2719
6. Kim, S.; Choi, S.; Park, C.; Jin, H.; *Thin Solid Films* **1999**, 347, (1-2), 155-160
7. Aparicio, M.; Jitianu, A.; Rodriguez, G.; Al-Marzoki, K.; Jitianu, M.; Mosa, J.; Klein, L. C. *Surface and Coatings Technology* **2017,** 315, 426-435.
8. Klein, L. C.; Jitianu, A., Encapsulating Battery Components with Melting Gels. In *Advances in Materials Science for Environmental and Energy Technologies III*, John Wiley & Sons, Inc.: 2014; pp 279-286.
9. Jaworek, A.; Sobczyk, A. T. *Journal of Electrostatics* **2008,** 66, (3–4), 197-219.
10. Lei, L.; Kovacevich, D. A.; Nitzsche, M. P.; Ryu, J.; Al-Marzoki, K.; Rodriguez, G.; Klein, L. C.; Jitianu, A.; Singer, J. P. *ACS Applied Materials & Interfaces* **2018,** 10, (13), 11175-11188.
11. Klein, L. C.; Kallontzi, S.; Fabris, L.; Jitianu, A.; Ryan, C.; Aparicio, M.; Lei, L.; Singer, J. P. *Journal of Sol-Gel Science and Technology* **2018**.
12. Schmidt, H. *Journal of Non-Crystalline Solids* **1988,** 100, (1), 51-64.
13. Danks, A. E.; Hall, S. R.; Schnepp, Z. *Materials Horizons* **2016,** 3, (2), 91-112.
14. Ohshima, T.; Matsumoto, M.; Miyata, T.; Uragami, T. *Macromolecular Chemistry and Physics* **2005,** 206, (16), 1638-1647.
15. Sanchez, C.; Julian, B.; Belleville, P.; Popall, M. *Journal of Materials Chemistry* **2005,** 15, (35-36), 3559-3592.
16. Matsuda, A.; Sasaki, T.; Hasegawa, K.; Tatsumisago, M.; Minami, T. *Journal of the American Ceramic Society* **2001,** 84, (4), 775-780.
17. Jitianu, A.; Amatucci, G.; Klein, L. C. *Journal of the American Ceramic Society* **2009,** 92, (1), 36-40.
18. Jitianu, A.; Gonzalez, G.; Klein, L. C. *Journal of the American Ceramic Society* **2015,** 98, (12), 3673-3679.
19. Jitianu, A.; Doyle, J.; Amatucci, G.; Klein, L. C. *Journal of Sol-Gel Science and Technology* **2010,** 53, (2), 272-279.
20. Brinker, C. J.; Scherer, G. W., *Sol-gel science: the physics and chemistry of sol-gel processing*. Academic press: 2013.
21. Husing, N.; Hartmann, S., Inorganic-Organic Hybrid Porous Materials. In *Hybrid nanocomposites for nanotechnology*, Merhari, L., Ed. Springer: 2009; pp 131-171.
22. Klein, L. C.; Jitianu, A. *Journal of Sol-Gel Science and Technology* **2010,** 55, (1), 86-93.

23. Gambino, L.; Jitianu, A.; Klein, L. C. *Journal of Non-Crystalline Solids* **2012,** 358, (24), 3501-3504.
24. Klein, L. C., Sol-Gel Coatings. In *Thin film processes II*, Kern, W., Ed. Academic press: 2012; Vol. 2, pp 501-520.
25. Blumberg, L. N.; Gursky, J. C.; Stein, P. C., *Electrospraying of Thin Targets*. Los Alamos Scientific Laboratory: 1962.
26. Gaskell, S. J. *Journal of mass spectrometry* **1997,** 32, (7), 677-688.
27. Merrill, M. H.; Pogue, I. I. I. W. R.; Baucom, J. N. *Journal of Micro and Nano-Manufacturing* **2015,** 3, (1), 011003-011003.
28. Gañán-Calvo, A. M.; Dávila, J.; Barrero, A. *Journal of Aerosol Science* **1997,** 28, (2), 249-275.
29. Weiss, F. M.; Topper, T.; Osmani, B.; Peters, S.; Kovacs, G.; Muller, B. *Adv. Electron. Mater.* **2016,** 2, (5), 8.
30. Yeo, L. Y.; Gagnon, Z.; Chang, H.-C. *Biomaterials* **2005,** 26, (31), 6122-6128.
31. Yeo, L. Y.; Lastochkin, D.; Wang, S.-C.; Chang, H.-C. *Physical Review Letters* **2004,** 92, (13), 133902.
32. Yang, W.; Lojewski, B.; Wei, Y.; Deng, W. *Journal of Aerosol Science* **2012,** 46, 20-33.
33. Moerman, R.; Frank, J.; Marijnissen, J. C. M.; Schalkhammer, T. G. M.; van Dedem, G. W. K. *Analytical Chemistry* **2001,** 73, (10), 2183-2189.
34. Hinaut, A.; Pawlak, R.; Meyer, E.; Glatzel, T. *Beilstein Journal of Nanotechnology* **2015,** 6, 1927-1934.
35. Hu, H.; Singer, J. P.; Osuji, C. O. *Macromolecules* **2014,** 47, (16), 5703-5710.
36. Hu, H.; Toth, K.; Kim, M.; Gopalan, P.; Osuji, C. O. *MRS Communications* **2015,** 5, (02), 235-242.
37. Choo, Y.; Hu, H.; Toth, K.; Osuji, C. O. *Journal of Polymer Science Part B: Polymer Physics* **2016,** 54, (2), 247-253.
38. Hu, H.; Toth, K.; Kim, M.; Gopalan, P.; Osuji, C. O. *MRS Communications* **2015,** 5, (2), 235-242.
39. Kim, J.-S.; Chung, W.-S.; Kim, K.; Kim, D. Y.; Paeng, K.-J.; Jo, S. M.; Jang, S.-Y. *Advanced Functional Materials* **2010,** 20, (20), 3538-3546.
40. Rietveld, I. B.; Kobayashi, K.; Yamada, H.; Matsushige, K. *Soft Matter* **2009,** 5, (3), 593-598.
41. Guo, Q.; Mather, J. P.; Yang, P.; Boden, M.; Mather, P. T. *PLOS ONE* **2015,** 10, (6), e0129960.
42. Novak, S.; Lin, P.-T.; Li, C.; Borodinov, N.; Han, Z.; Monmeyran, C.; Patel, N.; Du, Q.; Malinowski, M.; Fathpour, S.; Lumdee, C.; Xu, C.; Kik, P. G.; Deng, W.; Hu, J.; Agarwal, A.; Luzinov, I.; Richardson, K. *JoVE* **2016**, (114), e54379.
43. Novak, S.; Johnston, D. E.; Li, C.; Deng, W.; Richardson, K. *Thin Solid Films* **2015,** 588, 56-60.
44. Chavhan, M. P.; Ganguly, S. *Industrial & Engineering Chemistry Research* **2016,** 55, (38), 10073-10083.
45. Leeuwenburgh, S.; Wolke, J.; Schoonman, J.; Jansen, J. *Journal of Biomedical Materials Research Part A* **2003,** 66A, (2), 330-334.
46. Siebers, M. C.; Walboomers, X. F.; Leeuwenburgh, S. C. G.; Wolke, J. G. C.; Jansen, J. A. *Biomaterials* **2004,** 25, (11), 2019-2027.

47. Kim, J.-Y.; Kim, E.-K.; Kim, S. S. *Journal of Colloid and Interface Science* **2013,** 392, 376-381.
48. Kim, J. W.; Yamagata, Y.; Kim, B. J.; Higuchi, T. *Journal of Micromechanics and Microengineering* **2009,** 19, (2), 025021.
49. Al-Milaji, K. N.; Zhao, H. *Applied Surface Science* **2017,** 396, 955-964.
50. Burkarter, E.; Saul, C. K.; Thomazi, F.; Cruz, N. C.; Roman, L. S.; Schreiner, W. H. *Surface and Coatings Technology* **2007,** 202, (1), 194-198.
51. Coll, A.; Bermejo, S.; Martin, I.; Ortega, P.; Alcubilla, R. *Microelectronic Engineering* **2016,** 153, 20-23.
52. Hou, X.; Choy, K.-L. *Surface and Coatings Technology* **2004,** 180–181, 15-19.
53. Krella, A. K.; Sobczyk, A. T.; Krupa, A.; Jaworek, A. *Mechanics of Materials* **2016,** 98, 120-133.
54. Singh, S.; Meena, V. K.; Sharma, M.; Singh, H. *Materials & Design* **2015,** 88, 278-286.
55. Hwang, D.; Lee, H.; Jang, S.-Y.; Jo, S. M.; Kim, D.; Seo, Y.; Kim, D. Y. *ACS Applied Materials & Interfaces* **2011,** 3, (7), 2719-2725.
56. Hu, H.; Choo, Y.; Feng, X.; Osuji, C. O. *Macromolecular Rapid Communications* **2015,** 36, (13), 1290-1296.
57. Ellis, N.; Yurteri, C. U.; Ruud van Ommen, J. *Chemical Engineering Journal* **2012,** 181–182, 798-805.
58. Morozov, V. N., Electrospray Deposition of Biomolecules. In *Nano/Micro Biotechnology*, Endo, I.; Nagamune, T., Eds. Springer Berlin Heidelberg: Berlin, Heidelberg, 2010; pp 115-162.
59. Bodnár, E.; Rosell-Llompart, J. *Journal of Colloid and Interface Science* **2013,** 407, (0), 536-545.
60. Lenggoro, I. W.; Lee, H. M.; Okuyama, K. *Journal of Colloid and Interface Science* **2006,** 303, (1), 124-130.
61. Morozov, V.; Morozova, T.; Kallenbach, N. *International Journal of Mass Spectrometry* **1998,** 178, (3), 143-159.
62. Welle, A. M.; Jacobs, H. O. *Applied Physics Letters* **2005,** 87, (26), 263119.
63. Jitianu, A.; Doyle, J.; Amatucci, G.; Klein, L. C. *Proceedings MS&T* **2008**, 2171-2182.
64. Jitianu, A.; Kim, M.-S.; Andreescu, D.; Goia, D. V. *Journal of Nanoscience and Nanotechnology* **2009,** 9, (3), 1891-1896.
65. Jitianu, A.; Lammers, K.; Arbuckle-Kiel, G. A.; Klein, L. C. *Journal of Thermal Analysis and Calorimetry* **2012,** 107, (3), 1039-1045.
66. Jitianu, M.; Jitianu, A.; Stamper, M.; Aboagye, D.; Klein, L. C. *MRS Proceedings* **2013,** 1547, 81-86.
67. Picard, Q.; Akalonu, G.; Mercado, J.; Mosa, J.; Aparicio, M.; Klein, L.; Jitianu, A., *Electrodeposition of Hybrid Sol-Gel Glass Coatings on 304 Stainless Steel for Corrosion Protection*. 2018; Vol. 265, p 205-220.
68. Jitianu, A.; Cadars, S.; Zhang, F.; Rodriguez, G.; Picard, Q.; Aparicio, M.; Mosa, J.; Klein, L. C. *Dalton Transactions* **2017,** 46, (11), 3729-3741.
69. Aegerter, M. A.; Mennig, M., *Sol-gel technologies for glass producers and users*. Springer Science & Business Media: 2013.

70. Williams, M. L.; Landel, R. F.; Ferry, J. D. *Journal of the American Chemical society* **1955,** 77, (14), 3701-3707.
71. White, R. P. *Polymer Engineering & Science* **1974,** 14, (1), 50-57.
72. Recchia, S.; Zheng, J. Q.; Horner, S.; Pelegri, A. A. *Acta Mechanica* **2015,** 226, (12), 4149-4158.
73. Tenorio, M.; Pelegri, A. A. **2013**, (56444), V015T16A023.
74. Sullivan, D. J.; Taylor, P. A.; Pelegri, A. A. **2013**, (56215), V03AT03A020.
75. Recchia, S. S.; Pelegri, A.; Clawson, J. K.; Sahin, K.; Chasiotis, I.; Zheng, J. **2013**, (56383), V009T10A063.
76. Pelegri, A. A.; Huang, X. *Composites Science and Technology* **2008,** 68, (1), 147-155.
77. Huang, X.; Pelegri, A. A. *Composites Science and Technology* **2007,** 67, (7–8), 1311-1319.
78. Huang, X.; Pelegri, A. A. *Journal of Engineering Materials and Technology* **2003,** 125, (4), 361-367.
79. Singer, J. P.; Pelligra, C. I.; Kornblum, N.; Choo, Y.; Gopinadhan, M.; Bordeenithikasem, P.; Ketkaew, J.; Fatt Liew, S.; Cao, H.; Schroers, J.; Osuji, C. O. *Microsystems & Nanoengineering* **2015,** 1, 15040.
80. Lawn, B., *Fracture of brittle solids*. Cambridge university press: 1993.
81. Hutchinson, J. W.; Suo, Z., Mixed Mode Cracking in Layered Materials. In *Advances in Applied Mechanics*, John, W. H.; Theodore, Y. W., Eds. Elsevier: 1991; Vol. Volume 29, pp 63-191.
82. Seung Hwan, K.; Jaewon, C.; Nico, H.; Koo Hyun, N.; Costas, P. G. *Journal of Micromechanics and Microengineering* **2010,** 20, (12), 125010.
83. Li, J.; Ye, F.; Vaziri, S.; Muhammed, M.; Lemme, M. C.; Östling, M. *Advanced Materials* **2013,** 25, (29), 3985-3992.
84. Li, J.; Naiini, M. M.; Vaziri, S.; Lemme, M. C.; Östling, M. *Advanced Functional Materials* **2014,** 24, (41), 6524-6531.
85. Santora, B. P.; Gagné, M. R.; Moloy, K. G.; Radu, N. S. *Macromolecules* **2001,** 34, (3), 658-661.
86. Henriksen, T.; Juhler, R. K.; Svensmark, B.; Cech, N. B.; *Journal of the American Society for Mass Spectrometry* **2005**, 16, (4), 446-455.
87. Gamboa, A. R**.;** Nitzsche, M. P.; Saro-Cortes, V.; Ma, T.; Lei, L.; Singer, J. P.; *MRS Advances* **2018**, 3, (18), 977-982.
88. Zeleny, J.; *Physical Review* **1914,** 3, (2), 69-91.
89. Hench, L. L.; West, J. K.; *Chemical Reviews* **1990**, 90, (1), 33-72.
90. Klein, L. C.; Garvey, G. J.; *Journal of Non-Crystalline Solids* **1980,** 38, (1), 45-50.